Atrane Precursors in the One-Pot Surfactant-Assisted Synthesis of High Zirconium Content Porous Silicas

Jamal El Haskouri,[†] Saúl Cabrera,[‡] Carmen Guillem,[†] Julio Latorre,[†] Aurelio Beltrán,[†] Daniel Beltrán,[†] M. Dolores Marcos,*[,§] and Pedro Amorós*[,†]

Institut de Ciència dels Materials de la Universitat de València (ICMUV), P.O. Box 2085, 46071 Valencia, Spain, Laboratorio de Sólidos y Química Teórica, Instituto de Investigaciones Químicas UMSA, Cota-Cota, Calle nº 27, La Paz, Bolivia, and Departamento de Química, Universidad Politécnica de Valencia, Camino de Vera s/n, 46071 Valencia, Spain

Received May 14, 2002. Revised Manuscript Received September 16, 2002

A diversity of zirconium-containing porous silicas of the MCM-41 type (Zr−MCM-41, ∞ ≥ Si/Zr ≥ 0.33) has been synthesized from aqueous solution using a cationic surfactant (CTABr = cetyltrimethylammonium bromide) as the structural directing agent, and starting from molecular atrane complexes of Zr and Si as precursors. Atrane inertness toward hydrolysis allows harmonization of the reactivity of the Zr and Si species, which in turn avoids subsequent phase segregation and results in chemically very homogeneous materials. Materials characterization by XRD, TEM, and N_2 adsorption−desorption isotherms shows that all the prepared Zr−MCM-41 solids have high surface area and unimodal narrow pore size distribution, whereas their pore packing motives range from ordered hexagonal to wormhole-like arrays depending on the Zr content. The study of the local environment of the Zr atoms in these solids has been approached by means of spectroscopic techniques (IR, UV−vis, and NMR).

Introduction

Zirconia catalysts are finding widespread use due to both their moderate acidity and their oxidizing capability.[1] However, the possibility of industrial applications is limited because these materials generally show low surface area (lower than 50 m^2/g) and no size selectivity.[2,3] One usual way to overcome the first problem lies in supporting zirconia on high surface oxides, mainly silica.[4−6] The resulting catalysts display strong acidity and show satisfactory activity in a diversity of organic reactions (alcohol dehydration, alkene isomerization, and cumene dealkylation).[7,8] In contrast, the limitation associated with the lack of size selectivity remains a major trouble area. Two synthetic routes have been explored to resolve it: the direct preparation of porous zirconia[9] or, alternatively, the synthesis of molecular sieves (zeolite or porous materials) which incorporate Zr atoms into their frameworks. This last strategy seems to be the most promising one, given that pure porous zirconia (i.e., after template removal) becomes unstable and has relatively low surface area. Thus, there are reports on microporous materials, such as Zr−ZSM-5 or Zr−ALPO-5,[10,11] which simultaneously display high surface area and size selectivity. (The Zr active centers are only accessible to molecules with small kinetic diameter.) Also, to extend the zirconia catalytic capabilities to other larger organic substrates used in fine chemistry, the feasibility of incorporating Zr atoms into mesoporous silica has been explored by implementing one-pot or postsynthesis grafting methods. Indeed, Zr atoms have been introduced into the framework of ordered (MCM-41[12−15] and MCM-48[16]) and disordered (HMS)[17−19] mesoporous silicas. These solids combine high surface area (usually higher than 800 m^2/g) and size selectivity, but the synthetic procedures used severely affect the catalytic performances of the resulting materials.

* Authors to whom correspondence should be addressed. Phone: +34-96-3983617. Fax: +34-96-3983633. E-mail: pedro.amoros@uv.es; mmarcos@upvnet.upv.es.

[†] ICMUV.

[‡] Instituto de Investigaciones Químicas UMSA.

[§] Universidad Politécnica de Valencia.

(1) Tanabe, K.; Misono, M.; Ono, Y.; Hattori, H. *Stud. Surf. Sci. Catal.* **1989**, *51*, 1.
(2) Tanabe, K.; Yamaguchi, T. *Catal. Today* **1994**, *20*, 185.
(3) Yamaguchi, T. *Catal. Today* **1994**, *20*, 199.
(4) Gao, X.; Fierro, J. L. G.; Wachs, I. E. *Langmuir* **1999**, *15*, 3169.
(5) Dang, Z.; Anderson, B. G.; Amenomiya, Y.; Morrow, B. A. *J. Phys. Chem.* **1995**, *99*, 14437.
(6) Contescu, C. *J. Catal.* **1995**, *157*, 244.
(7) Bosman, H. J. M.; Kruissink, E. C.; Van der Spoel, J.; Van der Brink, F. *J. Catal.* **1994**, *148*, 660.
(8) Muller, J. B.; Rankin, S. E.; Ko, E. I. *J. Catal.* **1994**, *148*, 673.
(9) Ying, J. Y.; Mehnert, C. P.; Wong, M. S. *Angew. Chem., Int. Ed.* **1999**, *38*, 57.
(10) Dongare, M. K.; Singh, P.; Moghe, P. P.; Ratnasamy, P. *Zeolites* **1991**, *11*, 690.
(11) Dongare, M. K.; Sabde, D. P.; Shaikh, P. A.; Kamble, K. R.; Hegde, S. G. *Catal. Today* **1999**, *49*, 267.
(12) Wang, X. X.; Lefebvre, F.; Patarin, J.; Basset J. M. *Microporous Mesoporous Mater.* **2001**, *42*, 269.
(13) Chaudhari, K.; Bal, R.; Das, T. K.; Chandwadkar, A.; Srinavas, D.; Sivasanker, S. *J. Phys. Chem. B* **2000**, *104*, 11066.
(14) Occelli, M. L.; Biz, S.; Auroux, A. *Appl. Catal., A* **1999**, *183*, 231.
(15) Jones, D. J.; Jiménez-Jiménez, J.; Jiménez-López, A.; Maireles-Torres, P.; Olivera-Pastor, P.; Rodriguez-Castellón, E.; Rozière, J. *Chem. Commun.* **1997**, 431.
(16) Morey, M. S.; Stucky, G. D.; Schwarz, S.; Fröba, M. *J. Phys. Chem. B* **1999**, *103*, 2037.
(17) Tuel, A.; Gontier, S.; Teissier, R. *Chem. Commun.* **1996**, 651.
(18) Gontier, S.; Tuel, A. *Appl. Catal., A* **1996**, *143*, 125.
(19) Tuel, A. *Microporous Mesoporous Mater.* **1999**, *27*, 151.

10.1021/cm020131u CCC: $22.00
Published on Web 10/16/2002

Table 1. Selected Synthetic Parameters and Physical Properties of Zr−MCM-41 Porous Materials

sample	Si/Zr (precursor)	Si/Zr[a] (solid)	a_0[b] (Å) (as-synthesized)	a_0[b] (Å) (calcined)	shrinkage (Δ_0/Å)	S_{BET} (m^2g^{-1})	BJH pore (Å)	pore wall (Å)
1	∞	∞	43.94	39.20	4.74	1160.8	26.55	12.65
2	35	32(2)	43.94	38.61	5.33	907.0	25.10	13.51
3	25	24(2)	43.99	38.03	5.96	879.1	25.20	12.84
4	15	14(1)	44.05	37.99	6.06	902.1	25.10	12.89
5	10	10.0(4)	45.50	36.93	8.57	996.7	21.99	14.94
6	5	5.0(3)	48.53	36.40	12.13	687.5	22.15	14.25
7	3	3.0(3)	52.54	36.40	16.14	382.1	19.82	16.58
8	2	1.0(2)	46.33	31.07	15.26	141.7	<18.0	
9	1	0.33(8)	44.70	30.89	13.81	75.0	<18.0	

[a] Values averaged from EPMA of ca. 50 different particles (final porous materials). Spot area of ca. 1 μm and statistical esd's in parentheses. [b] Cell parameters calculated assuming a MCM-41 like hexagonal cell ($a_0 = 2*d_{100}/3^{1/2}$).

An important condition for having very active supported zirconia catalysts lies in site isolation: the Zr atoms must be isolated and well-dispersed throughout the silica network, thus avoiding the formation of ZrO_2 clusters.[20] In this sense, a major problem in the preparation of mixed oxides from aqueous media by sol−gel-related procedures is the unequal hydrolysis and condensation rates of the metal (or metalloid)-containing reagents. In the case we are dealing with, zirconium species usually hydrolyze faster than silicon precursors. In most cases, this results in partial segregation of ZrO_2 together with a decrease of the Zr/Si molar ratio in the resulting mixed oxide with respect to the initial (gel) composition. Insofar as the catalysts' performance substantially depends on their purity and chemical homogeneity, phase segregation must be avoided.

We report here on a new direct and reproducible surfactant-assisted procedure that has allowed us to prepare thermally stable Zr-containing porous silicas in which the Zr content in the framework can be modulated down to a minimum Si/Zr molar ratio value of 0.33. (In fact, the Zr-rich end compositions might be more properly referred to as Si-containing pororus zirconia.) The pore size of these materials is tuned from meso- to microporous as the Zr content increases. Our synthesis method takes advantage of using atrane complexing agents able to coordinate both Zr and Si and harmonize the reactivity of the resulting precursors.

Experimental Section

Synthesis. The method is based on the use of a cationic surfactant (CTAB = cetyltrimethylammonium bromide) as the structural directing agent (and, consequently, as porogen after template removal) and a complexing polyalcohol (2,2′,2″-nitriletriethanol or triethanolamine, hereinafter TEAH3) as the hydrolysis retarding agent (i.e., to balance the hydrolysis and condensation reaction rates of the Zr and Si precursor species).[21−24]

In a typical synthesis leading to the Si/Zr = 10 porous solid, 0.49 g of NaOH (12.25 mmol) was dissolved at 60 °C in a TEAH3 (20 mL, 150.68 mmol) solution containing 4.44 and 44.71 mmol of the zirconatrane and the silatrane derivatives of TEAH3[25,26] {in the form of M[TEA]$TEAH_2$ (M = Si, Zr), TEA and $TEAH_2$ meaning the fully deprotonated and diprotonated ligand, respectively}, respectively, and 4.23 g of CTAB (11.60 mmol). Then, 80 mL of water (4444.4 mmol) was slowly added with vigorous stirring. The mixture was allowed to age for 24 h at room temperature, resulting in the formation of a white mesostructured solid. This was then collected by filtration, washed with water and ethanol, and air-dried. To obtain the final mesoporous material, the as-synthesized solid was calcined (to thermally remove the surfactant) at 550 °C for 5 h under a static air atmosphere.

Summarized in Table 1 are the main synthesis variables and physical data concerning the Zr−MCM-41 porous materials prepared in this way. In all cases, the reagents molar ratio in the starting solution was adjusted to 2:*x*:6.74:0.52:0.55:199 Si:Zr:TEAH3:CTAB:NaOH:H_2O (x = 0, 0.06, 0.08, 0.13, 0.2, 0.4, 0.67, 1, 2).

The outstanding efficiency and versatility of the atrane route can be better appreciated as the complexity of the chemical system increases. Thus, this method makes possible incorporation into the mesoporous silica walls a wide variety of heteroelements and also facilitates the simultaneous introduction of several elements in a given silica matrix. By way of example, we present here the synthesis of a rich-zirconium ternary mesoporous oxide, Ti,Zr−MCM-41 (Si/Ti = 40, Si/Zr = 6). This solid was prepared as described above. The amounts of NaOH, TEAH3, CTAB, and water and the synthesis, aging, and thermal treatment conditions are maintained. The only modification consists of the addition of titanatrane together with the Zr and Si atrane complexes. Titanatrane complexes can be prepared from $Ti(OC_4H_9)_4$ and TEAH3 in a similar way as the Si and Zr derivatives.[26] In our case, the reagents molar ratio in the mother liquor was 2:0.05:0.33:6.74:0.52:0.55:199 Si:Ti:Zr:TEAH3:CTAB:NaOH:H_2O.

Physical Measurements. All solids were analyzed for Zr and Ti by electron probe microanalysis (EPMA) using a Philips SEM-515 instrument. Si/Zr molar ratio values averaged from EPMA data corresponding to ca. 50 different particles are summarized in Table 1. X-ray powder diffraction (XRD) data were recorded on a Seifert 3000TT $\theta-\theta$ diffractometer using Cu Kα radiation. Patterns were collected in steps of 0.02°(2θ) over the angular range 1−10°(2θ) for 25 s/step. To detect the presence of some crystalline bulk phase, additional patterns were collected with a bigger scanning step [0.05°(2θ)) over a wide angular range (10−70°(2θ)] and a lower acquisition time (10 s/step). TEM images were obtained by means of a Philips CM10 microscope operated at 120 kV. Room-temperature diffuse reflectance spectra were recorded (200−800 nm) using a Shimazdu UV−Vis 2501PC spectrophotometer. IR spectra (KBr pellets) were registered on a FTIR Perkin-Elmer 1750 spectrophotometer. ^{29}Si MAS NMR spectra were recorded on a Varian Unity 300 spectrometer operating at 79.5 MHz and using a magic-angle spinning speed of at least 4.0 kHz. All

(20) Flego, C.; Carluccio, L.; Rizzo, C.; Perego, C. *Catal. Commun.* **2001**, *2*, 43.
(21) Amorós, P.; Beltrán-Porter, A.; Beltrán-Porter, D.; Cabrera, S.; El Haskouri, J.; Marcos, M. D. Patent PCT/ES01/00122.
(22) El Haskouri, J.; Cabrera, S.; Caldés, M.; Alamo, J.; Beltrán-Porter, A.; Marcos, M. D.; Amorós, P.; Beltrán-Porter, D. *Int. J. Inorg. Mater.* **2001**, *3*, 1157.
(23) Prieto, O.; El Haskouri, J.; Beltrán, A.; Beltrán, D.; Marcos, M. D.; Amorós, P.; Choque, V.; Callisaya, E.; Luna, I.; Callejas, G.; Crespo, P.; Cabrera, S. *Rev. Boliv. Quím.* **2000**, *17*, 55.
(24) Cabrera, S.; El Haskouri, J.; Guillem, C.; Latorre, J.; Beltrán, A.; Beltrán, D.; Marcos, M. D.; Amorós, P. *Solid State Sci.* **2000**, *2*, 405.
(25) Kemmitt, T.; Al-Salim, N.; Mills, A. M.; Taylor, G.; Fenton, D.; Sutton, J. M.; Ono, K. Patent JP 2000264893.
(26) Naiini, A. A.; Ringgrose, S. L.; Su, Y.; Jacobson, R. A.; Verkade, J. *Inorg. Chem.* **1993**, *32*, 1290.

spectral measurements (IR, UV−Vis, NMR) were carried out under ambient conditions. Nitrogen adsorption−desorption isotherms were measured on a Micromeritics ASAP 2010 instrument, the samples being outgassed for 15 h at 130 °C and 10^{-6} Torr prior to measurement. Fast atomic bombardment (FAB) coupled to mass spectrometry (MS) analysis of the precursor solutions was performed to investigate the role played by TEAH3.

Results and Discussion

Synthesis Strategy. Alkoxides are very useful clean oxide precursors because, once displaced from the metal (or metalloid) environment by solvolysis, alcohol groups do not participate in subsequent processes (condensation) or can be easily removed from the solution. Indeed, this type of precursor has been widely used to prepare simple oxide mesoporous materials through surfactant-assisted procedures.[27,28] In this case, the main requirement to isolate an intermediate monophasic mesostructured solid is to achieve an adequate kinetic adjustment between the hydrolytic reactions of the precursor and the subsequent self-assembling processes (between the resulting inorganic moieties and the surfactant micelles). The situation changes when dealing with mesoporous mixed oxides. Unfortunately, the cohydrolysis approach to mixed oxides is plagued with problems related to the inherently different reactivity of the different precursors of the inorganic moieties, which frequently leads to phase segregation and the consequent isolation of undesired mixed phases.[24] Although with limited success, a technique that has been applied to solve this problem (i.e., to control the hydrolysis rate and condensation pathways) is based on the use of modified alkoxide precursors.[29] Alternatively, "single-source molecular precursors" (i.e., molecular precursors that simultaneously contains all the required oxide-forming elements) have also been explored.[30] Although this last polished approach has the advantage of ensuring an intimate mixture of the reactive elements from the initial preparative steps,[30] it presents a serious stoichiometric limitation: the composition of the final mixed oxide is conditional with respect to that of the precursor. Hence, for a given couple of elements, the final composition of the mixed oxide cannot be modified at will. On the other hand, in practice, this approach seems to be limited up to now to binary oxide systems.

Our synthesis strategy has been designed both to overcome problems associated with the great reactivity differences that characterize the most usual Zr and Si precursor species and to avoid, as far as possible, restrictions on the final stoichiometry. As shown below, triethanolamine (TEAH3) is used as a complexing agent able to keep the oxide-forming elements in homogeneous solution without undergoing phase segregation, even after water addition (a capability which depends on parameters such as apparent pH, temperature, and concentration).[31,32] Indeed, atrane complexes (i.e., complexes which include TEA-like species as ligands) are, in general, unstable but relatively inert toward hydrolysis. This feature of the atrane complexes chemistry has not been very well documented until now. However, the capability of TEA-like ligands to form amine-trialkoxo complexes by acting as anionic tripod ligands is well-known.[33] Hence, TEAH3 has been extensively used by ceramists to prepare heterometallic homogeneous solutions containing atrane complexes that can be utilized as pirolitic precursors of a diversity of bulk oxidic materials (e.g., PZTs, among other solids[34]). In contrast, only in recent times has the possible application of atrane complexes as hydrolytic precursors both of bulk and/or porous oxides been considered.[21,24,31,32,35] To analyze the specific role played by TEAH3 in the case we are dealing with, we have followed by means of mass-spectral analysis (FAB-MS) the formation and stabilization processes of the respective atrane complexes. This analysis has been carried out first on independent solutions containing the reagents required for the formation of the zirconatrane and silatrane derivatives of TEAH3[24−26] in which the molar concentrations of the reagents are very close to those used in the preparation of the Zr−MCM-41 porous materials described in this work: 2:7:0.5:*y* M:TEAH3:NaOH:H_2O (y = 0, 180). In the absence of water (y = 0), there are detected entities of different nuclearity in which TEAH3 displaces the starting alkoxide groups from the coordination spheres of the Si and Zr atoms (to give rise to the atrane complex species). Thus, the Si case, the majority fragment detected in anhydrous solution, is $SiNa(TEA)_2H_2^+$ (m/e = 345; %Rel = 100), which coexists with minor amounts of $Si(TEA)_2H_2$ (m/e = 322; %Rel = 30) and some more complex oligomers as $Si_2Na(TEA)_3H$ (m/e = 518; %Rel = 30) and $Si_3Na(TEA)_4^+$ (m/e = 691; %Rel = 18). The relative intensities have been calculated without considering the peaks associated with the dissolvent ($TEAH_3^+$ (m/e = 150) and $TEAH_3Na^+$ (m/e = 172)). In a similar way, the majority of Zr-containing species detected is $Zr(TEA)^+$ (m/e = 237; %Rel = 100%), while signals attributable to other zirconatrane fragments really display very low intensities ($Zr(TEA)_2H_2Na^+$ (m/e = 408; %Rel = 11%), $Zr(TEA)_3H_6ONa_2^+$ (m/e = 597, %Rel = 8%), $Zr_2(TEA)_3Na_2^+$ (m/e = 666; %Rel = 7%), and $Zr_3(TEA)_4Na^+$ (m/e = 880; %Rel = 4%)). After water addition (y = 180), both the Si and Zr atrane complexes remain in solution in the majority forms of $M(TEA)^+$ and M(TEA)OH species (i.e., no other more condensed species are FAB-MS detected prior to the respective oxide precipitation, ca. 5−10 min). In any case (y = 0, 180), the nature of the Si and Zr atrane complexes does not change apparently (FAB-MS) by simply mixing their solutions. In other words, although the formation to some extent of binary complexes (simultaneously containing both Si and Zr cations) cannot be discarded, it is not FAB-MS detected. Then, the precursor solution appears as mainly consisting of a random intimate mixture of independent Zr and Si molecular fragments. Hence, the role of TEAH3 is key for harmonizing the

(27) Corma, A. *Chem. Rev.* **1997**, *97*, 2373, and references therein.
(28) Schüth, F. *Chem. Mater.* **2001**, *13*, 3184.
(29) Brinker, G.; Scherer, G. *Sol Gel Science: The physics and chemistry of sol−gel processing*; Academic Press: New York, 1990.
(30) Kriesel, J. W.; Sander, M. S.; Don Tilley, T. *Chem. Mater.* **2001**, *13*, 3554.
(31) Cabrera, S.; El Haskouri, J.; Alamo, J.; Beltrán, A.; Beltrán, D.; Mendioroz, S.; Marcos, M. D.; Amorós, P. *Adv. Mater.* **1999**, *11*, 379.
(32) Cabrera, S.; El Haskouri, J.; Beltrán, A.; Beltrán, D.; Mendioroz, S.; Marcos, M. D.; Amorós, *Solid State Sci.* **2000**, *2*, 513.
(33) Verkade, J. G. *Acc. Chem. Res.* **1993**, *26*, 2711, and references therein.
(34) Das, R. N.; Pathak, A.; Pramanik, P. *J. Am. Ceram. Soc.* **1998**, *81*, 3357.

hydrolytic reactions which generate the inorganic entities involved in the self-assembling processes with the surfactant (to give surfactant−inorganic composite micelles, the elemental building blocks of the mesostructures). In this way, the atrane route allows easy modulation of the Zr relative content in the resulting mixed oxide along a wide compositional range, $\infty \geq$ Si/Zr ≥ 0.33 (see below). Such a lower limit value corresponds to a relative Zr content significantly higher than those previously reported in the literature by using surfactants or block copolymers as supramolecular templates.[12−19]

Characterization. We have used EPMA to assess the stoichiometry and chemical homogeneity of the samples, given that a principal objective of our work was to favor a good dispersion of the heteroelement into the inorganic walls of the resulting materials. EPMA data (see Table 1) show that all the reported samples are chemically homogeneous at the scale spot area. Hence, the solids can be considered as monophasic products, and segregation of crystalline ZrO_2 can be practically discarded even for the samples having the highest Zr contents (although formation of ZrO_2-like amorphous nanodomains should progress as the Zr content). This result is consistent with the absence of zirconia peaks in the high-angle region of the XRD patterns.

In the compositional range $\infty \geq$ Si/Zr ≥ 3, the Si/Zr molar ratio in the final solid is very close to that present in the mother solution. Only in the case of the solids prepared from the precursor solutions having the highest Zr contents (Si/Zr = 2 and 1), a certain increase in the Zr content is observed with regard to the starting solution composition. This fact indicates that there is no preferential incorporation of Zr or Si into the final network, at least up to Si/Zr = 3. This result is a consequence of the harmonization of the hydrolytic reaction rates of the Si and Zr species when starting from atrane precursors instead of conventional alkoxides. In contrast, when using TEOS and $Zr(OC_4H_9)_4$ as precursors and working in a rich water medium (as it occurs in our case), the results in ref 13 show that already there are deviations between the compositions of the initial gel and the final product at ca. Si/Zr = 50.

The symmetry and order degree of both the as-synthesized and final materials have been studied by XRD and TEM. Shown in Figure 1 are the XRD patterns corresponding to the prepared materials before (mesostructured) and after (porous) template removal. All materials display XRD patterns with at least one strong diffraction peak in the low-angle region, which is characteristic of mesostructured/porous materials. This peak usually is associated with the (100) reflection when a hexagonal cell (similar to that described in the case of MCM-41) is assumed.[36] Apart from this intense peak, we can observe three other resolved small reflections in the patterns of the materials whose Zr content is comprised in the $\infty \geq$ Si/Zr ≥ 10 range. These signals can be indexed to the (110), (200), and (210) reflections of the typical hexagonal cell, and their observation constitutes a clear probe of the existence of highly ordered hexagonal (H_o) pore systems. Although these last peaks are also observed in the XRD patterns of the calcined samples, their relative intensity and resolution slightly decrease after template removal. In contrast, the XRD patterns of the materials whose Zr content is in the range $5 \geq$ Si/Zr ≥ 3 display only one broad signal together with the intense (100) peak. This broad signal (which includes the unresolved (110) and (200) reflections) is characteristic of disordered hexagonal arrays (H_d). As occurs in the case of the materials with lower Zr content, the relative intensity of this band also decreases after calcination. Finally, in the case of the solids having the highest Zr contents (Si/Zr = 1 and 0.33), the XRD patterns include only the (100) reflection band, which now appears significantly broadened. This effect is even more pronounced in the case of the final porous solids. The observation of only one broad signal is associated with highly disordered wormhole-like (W) pore systems.[37] Therefore, the incorporation of Zr into the silica-based hexagonal mesoporous framework implies a progressive lowering of order in the pore array. An interesting feature is that the atrane route allows the highly ordered hexagonal symmetry along a compositional range (up to Si/Zr = 10), the results being significantly larger than in the case of related materials prepared by surfactant-assisted procedures using commercial alkoxides or inorganic salts, to be maintained.[14,15]

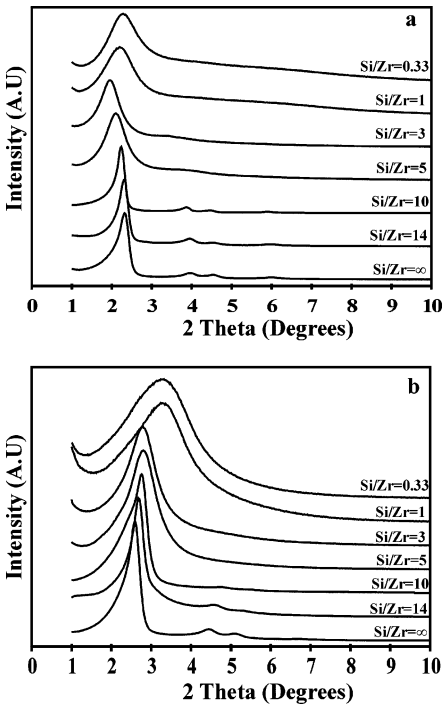

Figure 1. X-ray powder diffraction patterns of (a) as-synthesized (mesostructured) and (b) calcined (porous) Zr−MCM-41 materials.

The evolution of the cell parameters (see Table 1) supports the existence of the three compositional ranges mentioned above. Indeed, in the case of the mesostructured materials, the a_0 cell parameter value shows an initially increasing tendency as the Si/Zr ratio decreases, its value achieving a maximum at Si/Zr = 3. In fact,

(35) Sharma, P. K.; Varadan, V. V.; Varadan, V. K. *Chem. Mater.* **2000**, *12*, 2590.

(36) Kresge, C.; Leonowicz, M.; Roth, W.; Vartuli, J.; Beck, J. *Nature* **1992**, *359*, 710.

(37) Pauly, T. R.; Liu, Y.; Pinnavaia, T. J.; Billinge, S. J. L.; Rieker, T. R. *J. Am. Chem. Soc.* **1999**, *121*, 8835.

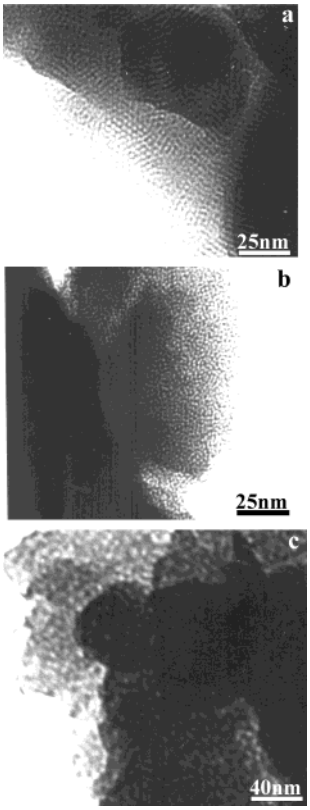

Figure 2. TEM images of selected Zr−MCM-41 porous (calcined) samples. (a) Si/Zr = 10; (b) Si/Zr = 5; (c) Si/Zr = 3.

the a_0 parameter remains practically unchanged in the range ∞ ≥ Si/Zr ≥ 14; then, its value slightly increases for the Si/Zr = 10 solid, and finally it markedly grows for solids whose composition is comprised in the range 5 ≥ Si/Zr ≥ 3. Such an evolution suggests that Zr atoms are effectively incorporated into the inorganic walls. In contrast, the value of the a_0 parameter pronouncedly decreases for the mesostructured materials having the highest Zr contents (Si/Zr = 1 and 0.33). A different behavior is observed in the case of the final (calcined) porous solids. Now, the a_0 parameter decreases as the Zr content increases along the entire compositional range. The evolution is gradual up to Si/Zr = 3; then, for the solids having the highest Zr content (Si/Zr = 1 and 0.33), the a_0 values are significantly lower. To understand this behavior, it is necessary to consider, together with the cell expansion due to the replacement of Si by Zr atoms, the strong network shrinkage, a consequence of the calcination process. As shown in Table 1, the contraction of the a_0 parameter upon calcination increases as the Si/Zr ratio decreases in the range ∞ ≥ Si/Zr ≥ 3. This significant shrinkage is similar to that observed in the case of pure ZrO_2 mesoporous solids prepared through surfactant-assisted procedures.[38]

TEM micrographs (Figure 2) fully correlate to XRD observations. The images confirm the evolution from H_0 to wormhole-like pore topologies. Solids having low zirconium contents (Si/Zr ≥ 10) show TEM images similar to that presented in Figure 2a, in which hexagonal order is detected. The Zr richest materials (Si/Zr ≤ 3) display wormhole-like pore systems similar to that observed in Figure 2c.

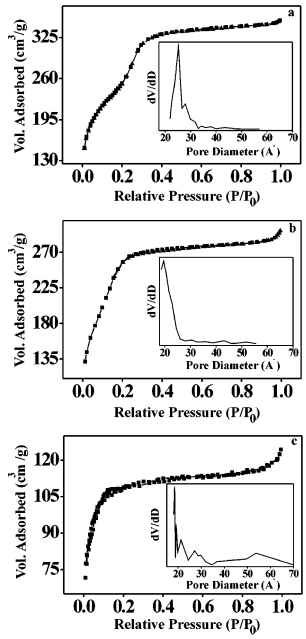

Figure 3. Representative N_2 adsorption−desorption isotherms of selected Zr−MCM-41 materials. (a) Si/Zr = 14; (b) Si/Zr = 10; (c) Si/Zr = 3. The pore size distributions (displayed in the insets) have been calculated by using the BJH model on the adsorption branch of the isotherms.

Nitrogen adsorption−desorption isotherm data (S_{BET}, BJH pore) are listed in Table 1, and selected curves are shown in Figure 3. Interestingly, the isotherms change in a gradual way from Type IV (IUPAC convention, pore diameter > 20 Å) to Type I (pore diameter < 20 Å), this indicating an evolution from meso- to microporous materials as the Zr content increases. Materials in the compositional range ∞ ≥ Si/Zr ≥ 10 originate from typical Type IV isotherms showing three adsorption stages. The first stage (P/P_0 < 0.2) can be related to a monolayer adsorption of N_2 on the porous walls. The second well-defined stage (0.2 < P/P_0 < 0.5) is related to capillary condensation of nitrogen inside the mesoporous. The absence of a hysteresis loop, as well as the sharp curvature along this second stage, suggests the existence of uniform and cylindrical channels throughout the materials. The third stage corresponds to adsorption in the near horizontal section for P/P_0 > 0.5, and it can be associated with multilayer adsorption on the external surface of the particles. Also, a small degree of additional adsorption is detected at high partial pressure. This last feature can be attributed to a certain proportion of interparticle textural porosity. As the Zr content increases, the beginning of the second stage shifts toward lower partial pressures, which indicates a progressive pore size reduction. The Zr richest materials (Si/Zr ≤ 5) show isotherms very similar to those typical of the Type I without hysteresis. However, the fact that nitrogen adsorption continues at P/P_0 > 0.2 suggests a certain contribution of both Type I and Type IV isotherms. This behavior has been previously observed in yttria−zirconia mesoporous solids.[39] The Si/

(38) Pacheco, G.; Zhao, E.; García, A.; Sklyarov, A.; Fripiat, J. J. *J. Mater. Chem.* **1998**, *8*, 219.

(39) Mamak, M.; Coombs, N.; Ozin, G. *J. Am. Chem. Soc.* **2000**, *122*, 8932.

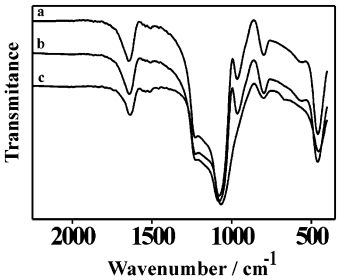

Figure 4. IR spectra (recorded under ambient conditions) of selected Zr−MCM-41 porous materials. (a) Si/Zr = 14; (b) Si/Zr = 10; (c) Si/Zr = 5.

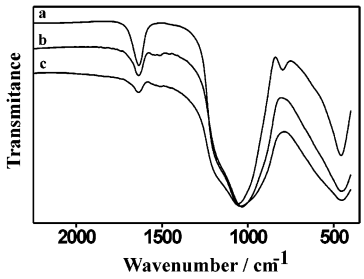

Figure 5. IR spectra (recorded under ambient conditions) of selected Zr−MCM-41 porous materials. (a) Si/Zr = 3; (b) Si/Zr = 1; (c) Si/Zr = 0.33.

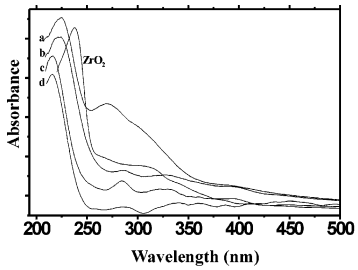

Figure 6. Diffuse reflectance UV−visible spectra (recorded under ambient conditions) of selected Zr−MCM-41 porous solids having different Si/Zr molar ratio: (a) 0.33; (b) 1; (c) 3; (d) 24. The spectrum of ZrO_2 is included as reference.

Zr ≤ 5 solids show averaged pore dimensions of ca. 16−22 Å, which are on the border between the microporous and mesoporous regimes.

Incorporation of Zr atoms has a significant effect on the BET surface area and pore size of the final materials (Table 1). As the Zr content increases up to Si/Zr = 10, the BET area remains practically unchanged (around 900−1000 m^2/g), although the pore size decreases from ca. 26.5 to 22.0 Å. However, the BET area significantly decreases for solids having high Zr contents (Si/Zr ≤ 5). In the case of the richest Zr derivatives (Si/Zr = 1 and 0.33), the surface area is very close to that observed for other porous oxides synthesized by using surfactants and polymers as supramolecular templates.[40,41] The thickness of the pore walls (estimated from XRD and porosity data) increases with the Zr content, which is in agreement with the incorporation of Zr atoms into the framework. This fact probably favors the comparatively high thermal stability of the title compounds. (The intensity and resolution of the XRD peaks remains practically unchanged when the solids are heated to 800 °C.)

Once confirmed that the prepared materials retain MCM-41 like structural arrays, we sought to gain insight on the location of the Zr centers and their environments by using spectroscopic techniques. In this matter, it must be noted that all our spectral measurements (IR, UV−Vis, NMR) were carried out under ambient conditions, where the surfaces might be hydrated. Notwithstanding, previous results in the literature concerning highly dispersed ZrO_2/SiO_2 related materials demonstrate that the Zr and Si environments are not altered by hydration.[4] The IR spectra of the mesoporous materials in the compositional range ∞ ≥ Si/Zr ≥ 5 (Figure 4) display, together with the bands at ca. 1090 and 1240 cm^{-1} (assigned to stretching Si−O−Si vibrations), an additional band at ca. 960 cm^{-1} that can be assigned to the stretching mode of SiO_4 entities bonded to Zr atoms (Si−O−Zr).[42,43] However, the pure silica MCM-41 material also exhibits a band at 960 cm^{-1} (probably due to silanol groups). Hence, the detection of this band cannot be used by itself as unambiguous proof for the isomorphous substitution of Zr for Si atoms. Notwithstanding, while in the compositional range ∞ ≥ Si/Zr ≥ 5 all the IR spectra show very similar features (the same number of bands at very close energy values and similar relative intensities), a clear spectral evolution is detected in the case of the Si/Zr ≤ 3 solids (Figure 5). Now, the resolution of the IR bands decreases as the Zr content increases, and the band at 960 cm^{-1} disappears or is included in the wide band centered at 1100 cm^{-1}. On the other hand, the deformation of the low-energy band (ca. 460 cm^{-1}) suggests some absorption in the 500−700-cm^{-1} range. According to the literature, this fact could be associated with Zr−O−Zr vibrations.[44] In fact, ZrO_2 displays up to four bands at 450, 500, 610, and 780 cm^{-1} in the studied spectral window. Taking into account all these data, it seems reasonable to assume that, in the ∞ ≥ Si/Zr ≥ 5 compositional range, Zr atoms are preferentially incorporated in tetrahedral sites isomorphously replacing Si atoms. In the Zr-rich materials (3 ≤ Si/Zr ≤ 0.33) there should coexist Si−O−Zr fragments and small (XRD silent) ZrO_2 domains.

UV−vis spectroscopy can offer additional information on the dispersion and environment of Zr atoms inside the inorganic walls. Shown in Figure 6 are the UV−vis spectra of some selected porous samples. In all cases, the spectra display an intense absorption band at ca. 210−217 nm. This band is exactly centered at 210 nm for solids whose composition is comprised in the range 35 ≥ Si/Zr ≥ 10, and it appears gradually shifted toward low-energy values as the Zr content increases (214, 215, and 217 nm for the Si/Zr = 3, 1, and 0.33 solids, respectively). Apart from this intense band, in the spectra of the materials whose Zr content is in the range 5 ≥ Si/Zr ≥ 0.33, we can observe additional small bands in the 250−350-nm range. According to previous work on meso- and microporous Zr-containing solids, the intense absorption band at ca. 210 nm can be attributed to a charge-transfer transition from an oxygen atom to

(40) Chen, H.; Shi, J. L.; Zhang, W. H.; Ruan, M. L.; Yan, D. S. *Chem. Mater.* **2001**, *13*, 1035.
(41) Kim, J. M.; Shin, C. H.; Ryoo R. *Catal. Today* **1997**, *38*, 221.
(42) Dang, Z.; Anderson, B. G.; Amenomiya, Y.; Morrow, B. A. *J. Phys. Chem.* **1995**, *99*, 14437.
(43) Boccuti, M. R.; Rao, K. M.; Zecchina, A.; Leofanti, G.; Petrini, G. *Stud. Surf. Sci. Catal.* **1989**, *48*, 133.
(44) Makarov, A, D.; Boreskov, G. K.; Dzisko, V. A. *Kinet. Katal.* **1961**, *2*, 84.

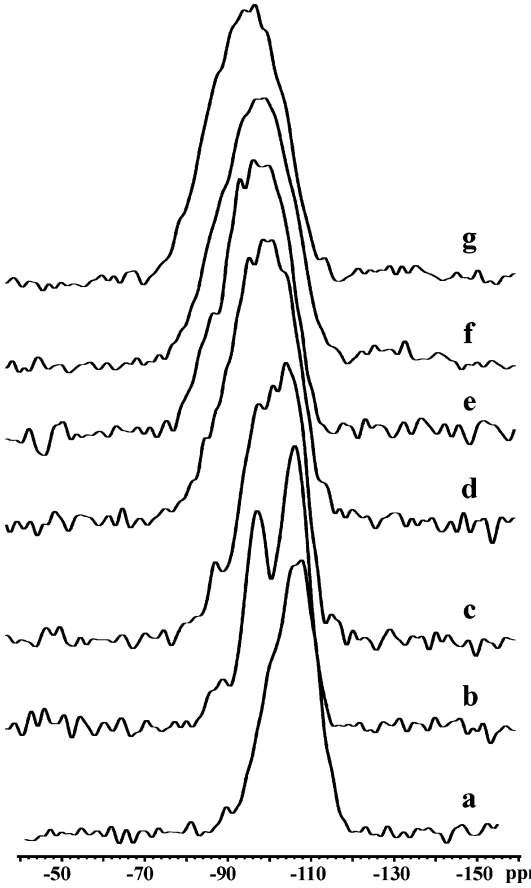

Figure 7. Evolution of the ^{29}Si MAS NMR spectra (recorded under ambient conditions) of Zr−MCM-41 materials with the zirconium content. (a) MCM-41; (b) Si/Zr = 24; (c) Si/Zr = 10; (d) Si/Zr = 5; (e) Si/Zr = 3; (f) Si/Zr = 1; (g) Si/Zr = 0.33.

an isolated Zr cation in a tetrahedral environment.[16] In the case of pure ZrO_2, where obviously there are no isolated Zr atoms, this ligand-to-metal charge transition band appears shifted toward lower energy (ca. 230−240 nm), and also there are observed additional bands in the 250−350-nm range. Thus, we can conclude that the above-mentioned shift of the high-energy intense signal from 210 to 217 nm (which occurs associated with a slight width increase) indicates a certain contribution of the zirconia absorption bands to the whole spectra. On the other hand, these observations suggest that all Zr atoms occupy isolated tetrahedral sites up to Si/Zr = 10. In the 5−0.33 Si/Zr range, a minor (but increasing) portion of the Zr atoms should be defining nanoscopic ZrO_2-like domains (Zr−O−Zr bonds). In short, UV−vis results suggest an optimum mixing degree of the Si and Zr atoms.

The good level of heteroelement dispersion achieved through the atrane route, even in the case of zirconium-rich samples, has been confirmed by ^{29}Si MAS NMR. Shown in Figure 7 are some selected spectra of the final porous materials. A certain controversy exists about the effects associated with the presence of Zr atoms in the ^{29}Si NMR spectra of mesoporous silicas. While Jones et al.[15] and Zhao et al.[45] have reported on modifications of the spectra with the Zr content, Wang et al.[12] and Chaudhari et al.[13] have concluded that the presence of Zr in the second coordination sphere of Si does not lead to measurable variations in the chemical shifts. As can be observed in Figure 7, there is a clear spectral evolution of the Si environments with the Zr content. While initially (MCM-41 pure silica) these are defined by only Si in the second coordination sphere [SiO_4, Si(4Si), and SiO_3OH, Si(3Si, OH)], they progressively incorporate Zr atoms [Si(4-nSi, nZr) and Si(3-nSi, OH, nZr)]. Indeed, the ^{29}Si NMR spectrum of the pure silica prepared by the atrane route displays a sharp and strong peak in the Q^4 [Si(4Si)] region ($\delta = -109$ ppm), and a shoulder in the Q^3 [Si(3Si, OH)] region ($\delta = -100$ ppm), this last indicating the presence of a low amount of silanol groups and the near absence of Q^2 [Si(2Si, 2OH)] centers. This fact can be attributed to the fast hydrolysis and condensation reactions of the silatrane precursors (leading to highly condensed networks) when compared to those of conventional alkoxides such as TEOS.[22,46] Then, as the Zr incorporation increases, a number of different signals appear at low chemical shifts (between −80 and −100 ppm). The spectrum of the Si/Zr = 24 solid displays two intense and resolved signals at −108 and −99 ppm and an additional small signal at −89 ppm. At first glance, this spectrum might be wrongly interpreted by incorrectly attributing these three signals to Q^4 [Si(4Si)], Q^3 [Si(3Si, OH)], and Q^2 [Si(2Si, 2OH)] silicon environments. However, a detailed comparison with the spectrum of the sample exempt from Zr clearly shows that the new signals must be associated with the Zr incorporation. According to the relevant literature on both amorphous bulk zirconium-containing silicas and crystalline zirconium silicates,[45,47,48] the significant growth of the signal at −99 ppm can be attributed to the presence of Si(3Si, 1Zr) environments. Hence, this signal includes Si(3Si, 1Zr) and Si(3Si, OH) silicon environments, and the signal at ca. −89 ppm is due to only Si(2Si, 2Zr) centers (taking into account that the existence of Q^2 [Si(2Si, 2OH)] environments is very unlikely in solids calcined at 550 °C). As the Zr content increases, a significant overlapping of the different signals occurs. This notwithstanding, a clear downfield shift of the whole spectrum is observed as the Zr content increases. Indeed, the intensity of the signal at −108 ppm, associated with Si(4Si) environments, clearly decreases as the Zr content increases and, simultaneously, a growth of the signals in the range −80 to −90 ppm is observed. Although a precise assignment of all the observed peaks is complicated due to the fact that is necessary to consider the simultaneous presence of Zr and OH groups in the second coordination sphere of Si atoms, it is possible to impute the signals around −100, −90, and −80 ppm to essentially Si(3Si, 1Zr), Si(2Si, 2Zr), and Si(1Si, 3Zr) silicon environments, respectively.

Ti−Zr−MCM-41 Mesoporous Solid. EPMA analyses carried out on ca. 50 different particles of the title compound show a high chemical homogeneity, with a good dispersion of the three heteroelements. This fact,

(45) Zhao, J.; Wu, D.; Sun, Y.; Zhang, Z.; Zhang, H.; Zhao, D. *Stud. Surf. Sci. Catal.* **2001**, *135*, 250.

(46) El Haskouri, J.; Cabrera, S.; Gutierrez, M.; Beltrán-Porter, A.; Beltrán-Porter, D.; Marcos, M. D.; Amorós, P. *Chem. Commun.* **2001**, 309.

(47) Bortum, A. I.; Bortum, L. N.; Clearfield, A. *Chem. Mater.* **1997**, *9*, 1854.

(48) Ferreira, P.; Ferreira, A.; Rocha, J.; Soares, M. *Chem. Mater.* **2001**, *13*, 355.

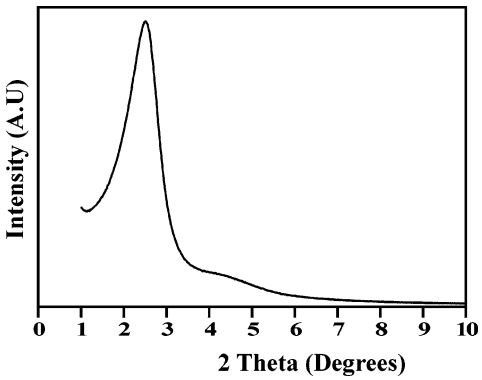

Figure 8. X-ray powder diffraction pattern of Ti,Zr−MCM-41 (Si/Ti = 40; Si/Zr = 6).

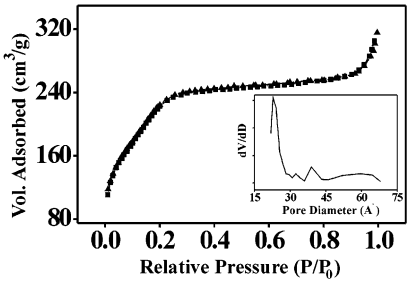

Figure 9. N_2 adsorption−desorption isotherm of Ti, Zr−MCM-41 (Si/Ti = 40; Si/Zr = 6).

together with the absence in the XRD pattern of the characteristic peaks of TiO_2 and ZrO_2, indicates the monophasic nature of Ti−Zr−MCM-41. The coincidence of the Si/M molar ratio values (Si/Ti = 40, Si/Zr = 6) in the starting solution and the final mesoporous material is indicative of the kinetically equilibrated hydrolysis and condensation reactions (for the three elements) that is achieved by using atrane precursors.

The low-angle XRD pattern (Figure 8) displays the intense (100) peak, and a wide and small signal that includes the (110) and (200) reflections, this indicating a disordered hexagonal pore organization. As expected, this spectrum is very similar to that observed for the Zr−MCM-41 (Si/Zr = 5) material. The N_2 adsorption−desorption isotherm (Figure 9) presents a well-defined adsorption step at intermediate pressures, which is characteristic of mesoporous materials. No hysteresis loop is observed, this indicating the preservation of a regular unimodal pore system. The BET surface area is 848 m^2/g. This relatively high value is intermediate between those observed for the Si/Zr = 10 and Si/Zr = 5 Zr−MCM-41 porous materials.

Concluding Remarks

Our work demonstrates that by using kinetically inert molecular precursors, it is possible to synthesize thermally stable Zr−MCM-41 porous silicas through cationic surfactant-assisted procedures. The atrane route allows the until now defined compositional range of the Zr−MCM-41 silicas (up to very high Zr content materials (Si/Zr = 0.33)) to be significantly extended. Consequently, the range of Zr−MCM-41 silicas displaying H_o ordered hexagonal arrays also becomes enlarged (up to the Si/Zr = 10 molar ratio). The pore size is modulated in a continuous way from meso- to microporous as the Zr content increases. Zr atoms preferently occupy tetrahedral sites in the inorganic network, although higher coordination environments are possible in the Zr richest materials. Taking into account the amorphous nature of the pore walls, it is not surprising that a glass-forming element (such as Zr) constitutes a good candidate for constructing (together with Si atoms) the continuous framework. According to Zachariasen's classification of glass-inserted elements,[49] Zr atoms can be considered as "intermediate" cations. This implies that Zr atoms could act, using the glass-maker jargon, both as "forming" (tetrahedral environment) and "modifier" cations. Up to Si/Zr = 10, all Zr atoms act as forming cations and the typical features of the MCM-41 (H_o) silicas are preserved. In the case of materials whose Zr content is in the range 5 ≥ Si/Zr ≥ 0.33, the Zr intermediate character becomes apparent, although tetrahedral sites are still preferred.

In light of our experience, we consider that the atrane route for producing mesoporous materials can be extended to the preparation of a diversity of polymetallic materials of catalytic interest.

Acknowledgment. This research was supported by the Ministerio de Ciencia y Tecnología (under Grants MAT2000-1387-C02-01 and PB98-1424-C02-01) and the Agencia Española de Cooperación Internacional.

CM020131U

(49) Zachariasen, W. *J. Am. Chem. Soc.* **1932**, *54*, 105.